GEOPHYSICS, VOL. 80, NO. 4 (JULY-AUGUST 2015); P. M43–M52, 14 FIGS., 1 TABLE.
10.1190/GEO2014-0374.1

Bayesian inversion of pressure diffusivity from microseismicity

Oleg V. Poliannikov[1], Michael Prange[2], Hugues Djikpesse[2], Alison E. Malcolm[3], and Michael Fehler[1]

ABSTRACT

We have considered the problem of using microseismic data to characterize the flow of injected fluid during hydraulic fracturing. We have developed a simple probabilistic physical model that directly ties the fluid pressure in the subsurface during the injection to observations of induced microseismicity. This tractable model includes key physical parameters that affect fluid pressure, rock failure, and seismic wave propagation. It is also amenable to a rigorous uncertainty quantification analysis of the forward model and the inversion. We have used this probabilistic rock failure model to invert for fluid pressure during injection from synthetically generated microseismicity and to quantify the uncertainty of this inversion. The results of our analysis can be used to assess the effectiveness of microseismic monitoring in a given experiment and even to suggest ways to improve the quality and value of monitoring.

INTRODUCTION

Hydraulic fracturing is the primary tool used to increase productivity of unconventional reservoirs (Ground Water Protection Council; ALL Consulting, 2009; Jones and Britt, 2009). A mixture of water and various additives is pumped under high pressure into the subsurface, fracturing the rock, and creating a network of fractures that provide pathways for hydrocarbons into the well (Charlez, 1997). Despite the ubiquitous use of hydraulic fracturing, the process often remains inefficient and costly due to the lack of comprehensive diagnostics to characterize the fracture network created. With no better alternative at hand, companies have no choice but to excessively fracture (and refracture) the rock at great cost to themselves (Vincent, 2010, 2012; LaFollette et al., 2013). Just a few important components contributing to the total cost of fracturing are as follows: water and proppant usage, pump trucks, water disposal, and public concern about triggered seismicity. All of these costs would be partially mitigated by a better understanding of the relationship between the fluid flow during the injection and the observed microseismic data. This understanding would also increase the value of microseismic monitoring and would likely lead to more efficient fracturing operations.

In this paper, we develop a probabilistic model that ties fluid pressure during injection to observed microseismicity. Our goal is twofold: to predict general patterns of microseismicity induced by the injected fluid and to invert for the pressure diffusivity of the subsurface from the observed microseismicity. The model we seek should therefore contain key components that control flow and rock failure, and it should also be computationally efficient to allow for inversion and uncertainty quantification. Presently, microseismicity is used in a somewhat simplistic way, in which estimated deterministic event locations are used to semiautomatically constrain fracture locations and geometry without any direct physical connection from the seismic events to flow (Maxwell, 2014). This fracture network may be further characterized by using past production data (history matching), and then it is used to predict production in the future. The success of models so obtained has been mixed, often yielding a large mismatch between model predictions and the actual field data (Cherian et al., 2011).

Shapiro and his collaborators (Shapiro et al., 2002, 2005a, 2005b) propose a physical model that directly ties fluid flow during injection with observed microseismic data. Theirs is a simple physical model that is based on the concept of linking the increasing pore pressure from fluid injection to the triggering of microseismic

Manuscript received by the Editor 11 August 2014; revised manuscript received 27 January 2015; published online 22 June 2015.
[1]Massachusetts Institute of Technology, Department of Earth, Atmospheric and Planetary Sciences, Earth Resources Laboratory, Cambridge, Massachusetts, USA. E-mail: poliann@mit.edu; fehler@mit.edu.
[2]Schlumberger-Doll Research, Cambridge, Massachusetts, USA. E-mail: prange@slb.com; hdjikpesse@gmail.com.
[3]Formerly Massachusetts Institute of Technology, Department of Earth, Atmospheric and Planetary Sciences, Earth Resources Laboratory, Cambridge, Massachusetts, USA; presently Memorial University of Newfoundland, Department of Earth Sciences, St. John's, Newfoundland, Canada. E-mail: amalcolm@mun.ca.

events using the Mohr-Coulomb theory of rock fracturing. As the pore pressure increases, the effective stress decreases, inducing microseismic triggering fronts. This theory predicts that the first event time t for microseismic events occurring a distance r from the injection well will lie on the level sets of r^2/t. They demonstrate that this prediction is born out in the field for microseismic observations in crystalline rock for geothermal stimulation (Shapiro et al., 2002, 2005a, 2005b) and in virtually impermeable shales for unconventional hydrocarbon stimulation (Hummel and Shapiro, 2013). This theory may be extended to predict not only the microseismic triggering fronts (the first events at a given distance), but also the statistics of events that occur after this front, including predictions of moment magnitude.

We propose a Bayesian reformulation of this model that accounts for the (typically large) uncertainties associated with rock cohesion, rock friction, and the maximum and minimum stresses of the formation, which are dominant factors controlling induced rock failure and the associated microseismicity. The probabilistic nature of the new model coupled with its relative simplicity is key for solving inverse problems and quantifying the uncertainty of the solution. By design, this model allows better use of microseismicity, going far beyond approximating fracture locations and geometry.

The uncertainty analysis provides insight into the relationship between the observed microseismicity and the hydraulic diffusivity, and it is likely to prove useful in many practical situations. When a large uncertainty is found in the inverted flow parameters (likely due to poorly known subsurface parameters), this both quantifies the confidence we have in the results and may hint at ways to improve that confidence.

This paper is organized as follows" In the "Rock failure model background" section, we describe the model for the distribution of fluid pressure during the injection and review the Mohr-Coulomb theory of rock failure and induced seismicity. The "Probabilistic rock failure model" section presents our new probabilistic model that can be used to predict microseismicity accounting for uncertainty in parameters that control rock failure. In the "Probabilistic inversion" section, we use our probabilistic model to show how to invert observed microseismic locations and origin times for the fluid pressure and quantify the uncertainty of the inversion. In the "Event location uncertainty" section, we discuss how to account for the uncertainty in the locations and times of a microseismic event, which is always present in field applications. In the "Discussion" section, we examine the applicability of the proposed approach and the remaining limitations. Finally, we summarize our work in the "Conclusions" section. For clarity, all notation used in this paper is summarized in Table 1, including the units used in all examples and figures.

Table 1. Table of symbols.

Symbol	Description	Units
A_s	Injection rate magnitude for constant rate injection	Pa/s
$F_{p_{\text{fail}}}(p)$	Cumulative distribution function of pressure at failure p_{fail}	None
$F_{t_{\text{fail}}(r_i\|\alpha)}(t)$	Cumulative distribution function of failure time $t_{\text{fail}}(r_i\|\alpha)$	None
$f_{p_{\text{fail}}}(p)$	Probability density function of pressure at failure p_{fail}	None
$f_{t_{\text{fail}}(r_i\|\alpha)}(t)$	Probability density function of failure time $t_{\text{fail}}(r_i\|\alpha)$, given that this time is finite	None
$\mathbb{P}[A]$	Probability of event A	None
$\mathbb{P}[A\|B]$	Probability of event A given event B	None
$P_{\text{fail}}(r\|\alpha)$	Probability of rock failure at distance r given diffusivity α	None
$p(r,t)$	Fluid pressure at distance r from the injection point, at time t	Pa
p_{fail}	Pressure necessary to affect rock failure	Pa
$p_{\max}(r\|\alpha)$	Maximal fluid pressure at distance r given diffusivity α	Pa
r	Radial distance from the injection well	m
$R(r,t)$	Injection rate as a function of distance r and time t	Pa/s
t	Time	s
s	Locations *and* origin times of all observed events	N/A
$t_{\text{fail}}(r\|\alpha)$	Time of rock failure at distance r given diffusivity α	s
$t_{\max}(r\|\alpha)$	Predicted time at which the fluid pressure at distance r is maximal	s
t_s	End of injection time	s
$\alpha(r)$	Fluid pressure diffusivity at distance r from the injection point	m^2/s
κ	Rock friction	None
σ_1	Maximum principal stress	Pa
σ_3	Minimum principal stress	Pa
σ_c	Rock cohesion	Pa

ROCK FAILURE MODEL BACKGROUND

Fluid pressure

Our model for hydraulic fracturing starts with the borehole fluid injection. We consider a radially symmetric medium with a source at the origin (Figure 1) (Shapiro et al., 2005a). We model the fluid pressure in the formation as an effective (upscaled) diffusion. Even when the rock matrix is virtually impermeable, fluid pressure may still diffuse at a larger scale through many connecting fractures (Shapiro et al., 2000). The upscaled effective diffusivity therefore accounts for possible fractures and fracture networks on the large scale, which is sufficient for a variety of field settings.

We assume that the fluid is injected into a medium with a nonhomogeneous diffusivity $\alpha(r)$ at a rate of $R(r,t)$. The pressure field $p(r,t)$ at distance r and time t is governed by the initial-value boundary-value problem (Shapiro et al., 2002, 2005a):

$$\begin{cases} \frac{\partial p(r,t)}{\partial t} = \nabla \cdot [\alpha(r) \nabla p(r,t)] + R(r,t), \\ p(r,0) = 0, \\ \frac{\partial}{\partial r} p(0,t) = 0, p(\infty,t) = 0. \end{cases} \quad (1)$$

Shapiro et al. (2002) propose that anisotropic diffusivity provides a better fit to effective flow through fractures, requiring a tensor-valued $\alpha(r)$ in equation 1, but for simplicity in this exposition, we use a scalar diffusivity.

We assume, for simplicity, that the injection is performed at the origin $r = 0$ with a constant rate of A_s from time $t = 0$ to $t = t_s$ as shown in Figure 2. The specific numbers used in the numerical experiments below are chosen for illustration purposes only. The problem defined by equation 1 can be solved analytically for a constant diffusivity, or numerically using a fast finite-difference code, for a general diffusivity, $\alpha(r)$. Because we are focusing here on the modeling of microseismic triggering fronts, we are interested in the maximum pressure as a function of distance r, $p_{\max}(r|\alpha)$, which can be attained at any time for a given diffusivity, $\alpha(r)$. We use the conditional notation from the probability theory here to emphasize the dependence on diffusivity $\alpha(r)$. This notation is convenient because the diffusivity will become a random variable later.

As a result of the injection, the fluid pressure within the medium $p(r, t)$ increases from $t = 0$ until it reaches its maximum value at some time $t_{\max}(r|\alpha) \geq t_s$, which depends on the location and the diffusivity, and then it drops and decays to zero as $t \to \infty$ as shown in Figure 3.

To find $t_{\max}(r|\alpha)$, we numerically solve for the extremum of the solution to the diffusion equation:

$$\frac{\partial}{\partial t} p(r, t|\alpha)\Big|_{t=t_{\max}(r|\alpha)} = 0. \quad (2)$$

The maximum pressure $p_{\max}(r|\alpha)$ attained at a distance r is calculated by plugging $t_{\max}(r|\alpha)$ into the solution to equation 1; i.e.,

$$p_{\max}(r|\alpha) \equiv p(r, t_{\max}(r|\alpha)|\alpha). \quad (3)$$

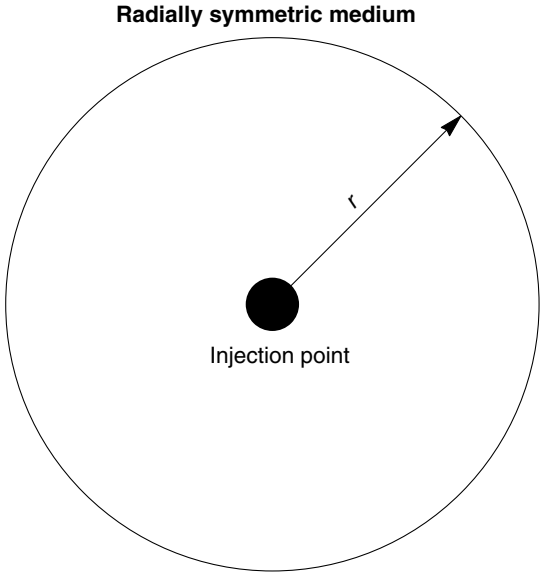

Figure 1. A radially symmetric medium is centered around the point of injection.

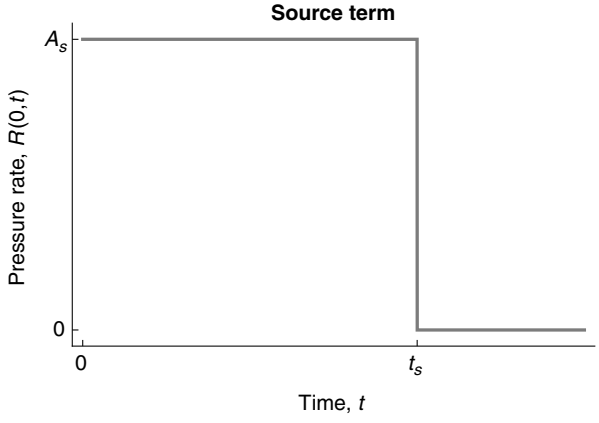

Figure 2. Injection rate at the location $r = 0$ that is the source term in equation 1. For expository simplicity, in all of our numerical examples we use $t_s = 1$ and $A_s = 1$.

Pressure at rock failure

Fluid injected as described above diffuses into a medium that can be characterized by a set of four model parameters. Specifically, consider a spatial grid $\{r_i\}_{i=1}^N$. At each location r_i, the medium can be described with four parameters that control rock failure: $m_i = \{\sigma_c(i), \kappa(i), \sigma_1(i), \sigma_3(i)\}$, where σ_c is the rock cohesion, κ is the rock friction, σ_1 is the maximum principal stress, and σ_3 is the minimum principal stress (Ottosen and Ristinmaa, 2005). Here, we will assume that all four parameters at all locations are statistically independent.

Time of failure

Let us first assume that the medium, including all four parameters mentioned above, is known, and we consider a location at distance r from the injection point. We will examine if there will be a failure at this location, and, if so, when.

According to the classical Mohr-Coulomb theory (Von Terzaghi, 1943), increasing the fluid pressure reduces the effective stress and, upon reaching a critical level, causes failure. This corresponds to the Mohr circle touching the Coulomb failure envelope at one point (Figure 4). The pressure level that is necessary to cause a rock failure at distance r_i will be called the pressure at failure and denoted $p_{\text{fail}}(i)$. From the requirement that the Mohr circle intersects the Coulomb envelope at exactly one point, after a bit of algebra we find that

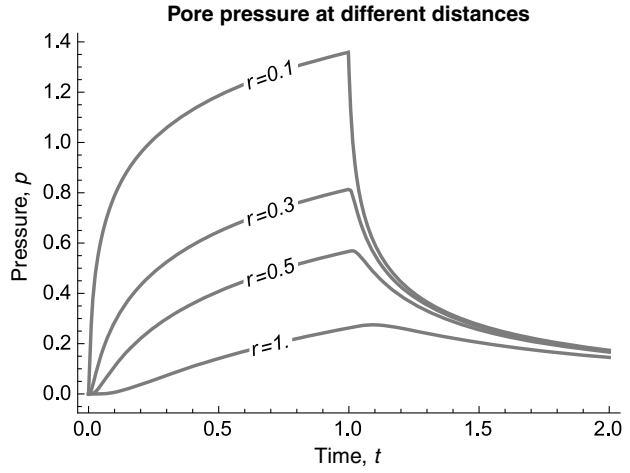

Figure 3. Sample pressure profiles that are solutions to equation 1, for a fixed diffusivity $\alpha(r) \equiv 1$ and different locations r.

$$p_{\text{fail}}(i) = \frac{\sqrt{\kappa(i)^2+1}(\sigma_3(i)-\sigma_1(i)) + \kappa(\sigma_3(i)+\sigma_1(i)) + 2\sigma_c(i)}{2\kappa(i)}. \quad (4)$$

Because the fluid pressure in the medium is predicted by equation 1 at all times, we can check if the failure will occur at $r = r_i$. A failure at distance r_i will only occur if the pressure reaches the failure pressure, $p_{\text{fail}}(i)$, at some time t; i.e.,

$$(\text{failure at } r = r_i) \Leftrightarrow (\exists t > 0 \quad p(r_i, t|\alpha) = p_{\text{fail}}(i)). \quad (5)$$

Because the maximum pressure attained at a fixed location is by definition no less than the pressure at this location at any given time,

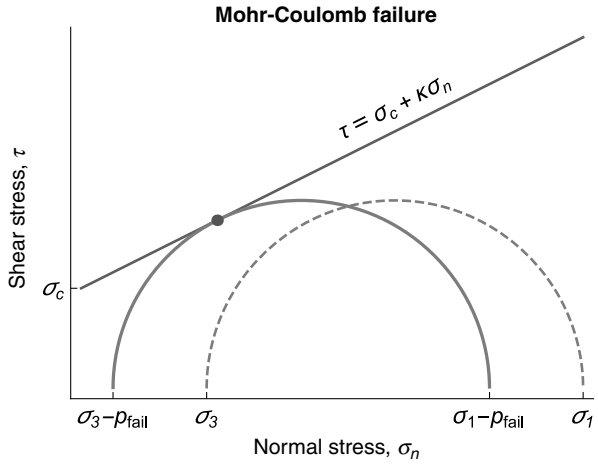

Figure 4. The pressure p rises until it reaches the level $p = p_{\text{fail}}$ when Mohr's circle touches the Coulomb failure envelope (straight line) and a failure occurs.

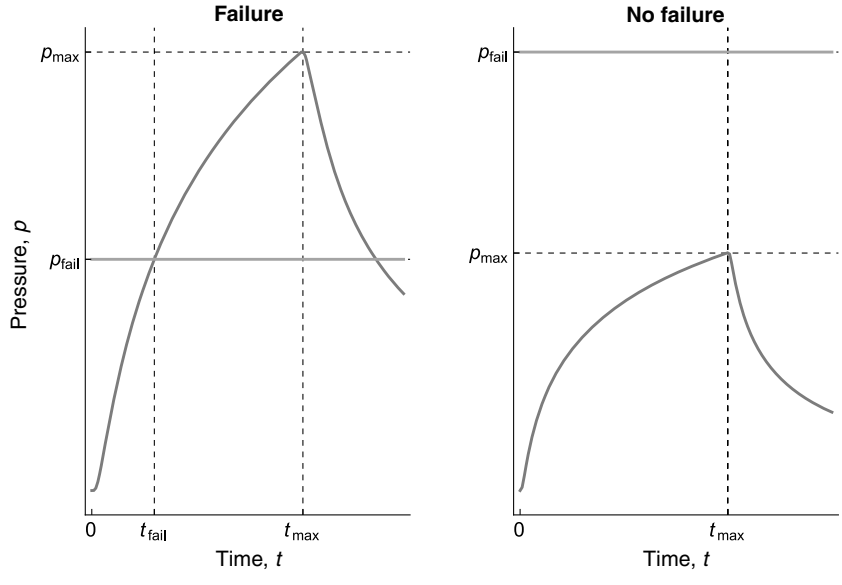

Figure 5. (a) A failure occurs if the pressure $p(r, t)$ at a given location r reaches the required level p_{fail}. The maximum pressure then by definition equals or exceeds this level. (b) If the pressure $p(r, t)$ never reaches the level p_{fail}, then no failure occurs at this location.

we can rewrite the failure condition in equation 5 as follows (see Figure 5a):

$$(\text{failure at } r = r_i) \Leftrightarrow (p_{\max}(r_i|\alpha) \geq p_{\text{fail}}(i)). \quad (6)$$

If the inequality in the right side of equation 6 is not satisfied because the pressure never rises to the required level, then no failure will occur (see Figure 5b). If the failure occurs at $r = r_i$, the time of failure will be

$$t_{\text{fail}}(r_i|\alpha) = \inf\{t > 0 | p(r_i, t|\alpha) = p_{\text{fail}}(i)\}. \quad (7)$$

Because the pressure at each location monotonously and continuously rises before reaching its peak and dropping off, it follows in the homogeneous case that failures occur in the r-t space along the curve

$$L_\alpha = \{(r, t) | p(r, t|\alpha) = p_{\text{fail}}\}, \quad (8)$$

where the pressure at failure p_{fail} is known.

This formulation immediately allows one to invert for the value of constant diffusivity from observed microseismicity by optimizing over α to fit a given failure curve L_α. Figure 6 shows the contours of the diffused pressure field (gray lines) and the associated induced microseismicity (black dots). We used a simple least-squares fit of the failure curve to recover the true diffusivity to almost machine precision.

PROBABILISTIC ROCK FAILURE MODEL

If the four parameters $\{\sigma_c, \kappa, \sigma_1, \sigma_3\}$ of the model and fluid pressure are deterministically known, then rock failure is directly linked to diffusivity, as is shown in the previous section. However, when the four parameters carry uncertainty and hence are described by probability distributions, a failure may or may not occur depending on a particular realization of these parameters. The probability distributions of the model parameters, called prior distributions (or priors) in Bayesian statistics, reflect our "prior" knowledge (with uncertainty) about the model, i.e., knowledge obtained from other measurements without any use of the observed microseismicity.

The inverted diffusivity is thus also an uncertain quantity with an associated probability density function. Given the prior distributions (priors) of the four model parameters, we can compute the distribution of the pressure at failure, p_{fail}, using Monte Carlo sampling and equation 4. In the numerical examples below, we use normal distributions with prescribed means and variances for the priors on the parameters, assuming independence between different locations r_i. The probability density function $f_{p_{\text{fail}}(i)} \times (p)$ of $p_{\text{fail}}(i)$ is then immediately computed from these assumptions and assumed known henceforth.

Denote the probability of failure at distance r_i as $P_{\text{fail}}(r_i|\alpha)$. The probability $P_{\text{fail}}(r_i|\alpha)$ is

specific to each given distance and diffusivity. It is computed as follows:

$$P_{\text{fail}}(r_i|\alpha) = \mathbb{P}[p_{\max}(r_i|\alpha) \geq p_{\text{fail}}(i)] = F_{p_{\text{fail}}(i)}(p_{\max}(r_i|\alpha)), \quad (9)$$

where $\mathbb{P}[\cdot]$ denotes probability and $F_{p_{\text{fail}}(i)}(p) \equiv \mathbb{P}[p_{\text{fail}}(i) \leq p] = \int_{-\infty}^{p} f_{p_{\text{fail}}(i)}(p')\mathrm{d}p'$ is the cumulative distribution function for $p_{\text{fail}}(i)$.

The time of failure $t_{\text{fail}}(r_i|\alpha)$ can either be finite, with probability $P_{\text{fail}}(r_i|\alpha)$, or it can be undefined (infinite), with probability $1-P_{\text{fail}}(r_i|\alpha)$ if failure never occurs at this distance. When this time is finite, it is a random variable whose distribution is described by a probability density function $f_{t_{\text{fail}}(r_i|\alpha)}(t)$. These distribution functions are computed as follows:

$$\begin{aligned} F_{t_{\text{fail}}(r_i|\alpha)}(t) &= \mathbb{P}[t_{\text{fail}}(r_i|\alpha) \leq t] \\ &= \mathbb{P}\Big[p_{\text{fail}}(i) \leq \max_{t' \in [0,t]} p(r, t'|\alpha)\Big] \\ &= F_{p_{\text{fail}}(i)}\Big(\max_{t' \in [0,t]} p(r, t'|\alpha)\Big). \end{aligned} \quad (10)$$

Recall that the diffused pressure, $p(r_i, t|\alpha)$, increases for $t \leq t_{\max}(r|\alpha)$ and decreases afterward. Therefore,

$$\max_{t' \in [0,t]} p(r, t'|\alpha) = \begin{cases} p(r, t|\alpha), & t \leq t_{\max}(r|\alpha), \\ p_{\max}(r|\alpha), & t > t_{\max}(r|\alpha). \end{cases} \quad (11)$$

Thus, we have for the cumulative distribution function $F_{t_{\text{fail}}(r_i|\alpha)}(t)$ for the time of failure,

$$F_{t_{\text{fail}}(r_i|\alpha)}(t) = \begin{cases} F_{p_{\text{fail}}(i)}(p(r,t|\alpha)), & t \leq t_{\max}(r|\alpha), \\ P_{\text{fail}}(r_i|\alpha), & t_{\max}(r|\alpha) < t < \infty, \\ 1, & t = \infty. \end{cases} \quad (12)$$

The conditional probability density function of the failure time given that failure can occur is

$$\begin{aligned} f_{t_{\text{fail}}(r_i|\alpha)}(t) &= \frac{1}{P_{\text{fail}}(r_i|\alpha)} \frac{\mathrm{d}}{\mathrm{d}t} F_{t_{\text{fail}}(r_i|\alpha)}(t) \\ &= \frac{1}{P_{\text{fail}}(r_i|\alpha)} \frac{\partial}{\partial p} F_{p_{\text{fail}}[(i)]}(p(r_i, t|\alpha)) \frac{\partial}{\partial t} p(r_i, t|\alpha) \\ &= \frac{f_{p_{\text{fail}}(i)}(p(r_i, t|\alpha)) \frac{\partial}{\partial t} p(r_i, t|\alpha)}{F_{p_{\text{fail}}(i)}(p_{\max}(r_i|\alpha))}, \end{aligned} \quad (13)$$

when $t \in [0, t_{\max}(r_i|\alpha)]$, and it is zero otherwise. In practice, many microseismic events are observed after $t_{\max}(r_i|\alpha)$, but because our focus here is on microseismic triggering fronts, these later events are not considered.

This framework allows us to forecast a probability distribution for microseismic events given the uncertain parameters $\{\sigma_c, \kappa, \sigma_1, \sigma_3\}$ in the subsurface. For each distance r_i across some a priori chosen grid, we can determine the probability of a failure $P_{\text{fail}}(r_i|\alpha)$ at the location r_i and, if applicable, the probability distribution of its time $f_{t_{\text{fail}}(r_i|\alpha)}(t)$. At each location, we first use the probability of failure to decide if there is a microseismic event; if there is an event, then we use the probability distribution of the time of failure to generate a random event time. By following this sampling procedure, we can obtain individual realizations of microseismicity (Figure 7).

PROBABILISTIC INVERSION

We formulate the inverse problem as follows: Given observed microseismicity,

$$s = \{(r_i, t_i)|t_i \in \mathbb{R} \cup \{\infty\}\}, \quad (14)$$

and a prior joint distribution of model parameters $m = (\sigma_1, \sigma_3, \sigma_c, \kappa)$ at all locations $\{r_i\}_{i=1}^{N}$, we would like to estimate the diffusivity $\alpha(r)$ in the medium. The observation $t_i = \infty$ corresponds to no event at distance r_i. We note that we could consider a more general problem of simultaneously inverting for all subsurface parameters $(\sigma_1, \sigma_3, \sigma_c, \kappa, \alpha)$ and examining the resulting trade-offs. However, in what follows, we concentrate on inverting for diffusivity α only while treating other parameters as known with some uncertainty.

To quantify the uncertainty of the inverted diffusivity, we will treat α as a random variable and attempt to recover its distribution given the observations and the priors. We will continue to assume that the subsurface parameters at different locations are statistically independent, and therefore, data points within s are independent, too.

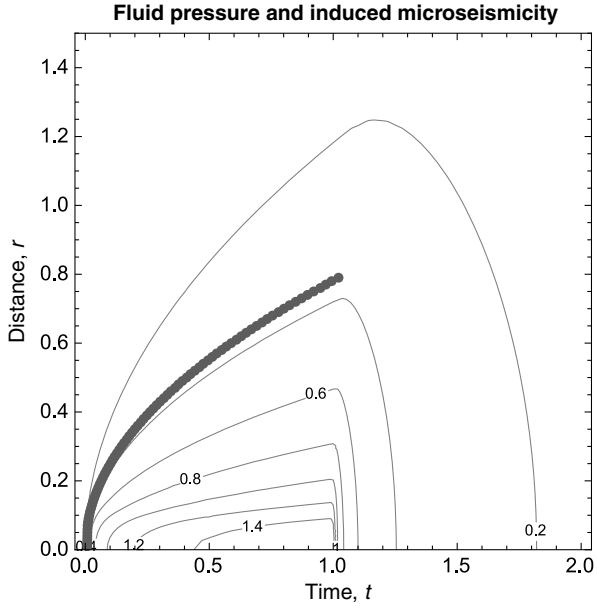

Figure 6. In a homogeneous medium, microseismic events (red dots) occur along the curve $\{(r, t)|p(r, t) = p_{\text{fail}}\}$. Various isobars are shown as thin gray lines. Given the observed microseismicity and the parameters controlling rock failure, the diffusivity can be estimated by fitting a curve given by equation 8 to the solution of the diffusion equation over a range of constant values of diffusivity α.

Applying Bayes' rule (Laplace, 1814), we get

$$\mathbb{P}[\alpha \in A | t \in T] = \frac{\mathbb{P}[t \in T | \alpha \in A]\mathbb{P}[\alpha \in A]}{\mathbb{P}[t \in T]}, \tag{15}$$

where $\mathbb{P}[\cdot \mid \cdot]$ denotes the conditional probability.

The likelihood function includes cases in which failure has occurred, and hence $t_i < \infty$, as well as cases where there has been no failure, and hence, $t_i = \infty$. More specifically,

$$\begin{aligned}\mathbb{P}[a \le t_i \le b|\alpha] &= \mathbb{P}[a \le t_i \le b, t_i < \infty|\alpha] \\ &= \mathbb{P}[a \le t_i \le b|t_i < \infty, \alpha]\mathbb{P}[t_i < \infty|\alpha] \\ &= \int_a^b f_{t_{\text{fail}}(r_i|\alpha)}(t_i)dt_i P_{\text{fail}}(r_i|\alpha),\end{aligned} \tag{16}$$

and

$$\mathbb{P}[t_i = \infty|\alpha] = 1 - P_{\text{fail}}(r_i|\alpha). \tag{17}$$

Treating the observations and nonobservations as measurements, the posterior density function for diffusivity is given by

$$\begin{aligned}f(\alpha|t_1, \ldots, t_N) \propto &\prod_{i'=1}^{N_{\text{events}}} f_{t_{\text{fail}}(r_i|\alpha)}(t_{i'})P_{\text{fail}}(r_{i'}|\alpha) \\ &\times \prod_{i'=N_{\text{events}}+1}^{N} (1 - P_{\text{fail}}(r_{i'}|\alpha)) \\ &\times f(\alpha),\end{aligned} \tag{18}$$

where $f(\alpha)$ is the prior and the index i' is chosen for convenience so that locations with events are counted first, and then locations without events are counted. We assume in the above derivation that all events have been registered at the receivers. Accounting for the probability of missing an event, e.g., due to its low magnitude, is left to future work.

In Figure 8, in thick line we show the posterior density function of the diffusivity α given the microseismicity shown in Figure 7. The true diffusivity $\alpha = 1$ has a high probability in this distribution.

This posterior distribution has an apparent "bias" because it is computed from a single random realization of induced microseismicity. If we consider multiple random realizations of microseismicity created using the forward model with the same parameters and compute posteriors for each realization (the thin gray curves in Figure 8), we can see that the peaks of these posterior distributions are scattered symmetrically around the true diffusivity value, $\alpha = 1$, suggesting no bias in the estimate.

Robustness of the posterior against various injections

We demonstrate the robustness of the proposed methodology by demonstrating the results of inversion for varying injection rates and durations of the injection. Figure 9 shows calculated posteriors for different choices of the injection duration. For each duration t_s, we generate a single realization of induced microseismicity and use it to invert for diffusivity. We see from the plot that the true diffusivity value has a high probability for all durations and the shapes of the distributions are very similar. This shows that the diffusivity and the associated uncertainty do not depend too much on the injection duration.

A similar test is performed by varying the injection rate A_s and computing the corresponding posterior distributions of the diffusivity. The results are shown in Figure 10. The true diffusivity is again recovered with a high probability, and the shapes of the posteriors appear quite similar. Note that when the injection rate is relatively low, the number of induced events is smaller. This results in a less constrained diffusivity inverse problem, which leads to a larger variance (width) of the diffusivity posterior.

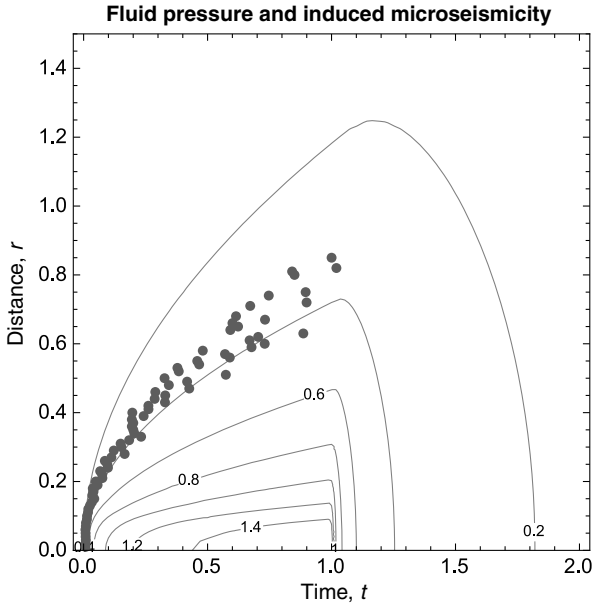

Figure 7. In a medium with uncertain parameters, microseismic events may or may not occur at given locations. The time of a microseismic event is also uncertain and governed by a probability distribution.

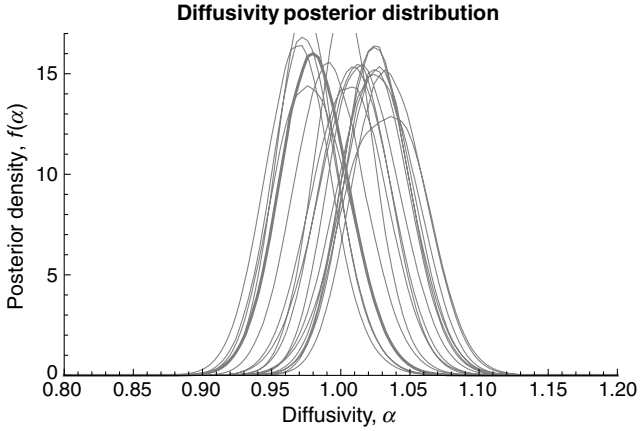

Figure 8. The posterior distribution of the diffusivity α given the observed microseismicity in Figure 7, the flat (completely uninformed) prior, and assumptions about the physical parameters of the medium are shown in the thick blue curve. Posteriors computed from other realizations of observed microseismicity are shown in the thin gray curves. The true diffusivity $\alpha = 1$ always remains inside the 3σ confidence interval, and the uncertainty is explicitly quantified.

Nonhomogeneous diffusivity

Now consider a nonhomogeneous example in which the diffusivity assumes one value α_1 near the borehole and another value α_2 away from the borehole. This is similar to a situation described by Suarez-Rivera et al. (2013a, 2013b). More precisely,

$$\alpha(r) = \begin{cases} \alpha_1, & r \le R, \\ \alpha_2, & r > R, \end{cases} \tag{19}$$

where $R = 0.5$ is assumed to be known. Figure 11 shows this setup. The water is pumped in the borehole centered at $r = 0$, resulting in induced microseismicity. For illustration purposes, we will assume no uncertainty in all parameters except the minimum stress σ_3. We will vary the uncertainty in σ_3 to show its effect on forecast microseismicity as well as on the uncertainty in the inverted diffusivities. Although σ_2 is typically the most uncertain of the principle stresses, it is σ_3 that controls the fracture orientation, and as such it is a parameter of great interest in a fracturing problem, which is why we chose it for this synthetic example.

Because the diffusivity α is no longer spatially homogeneous, we set $\alpha = (\alpha_1, \alpha_2)$ to be a vector of unknown diffusivities. We continue to assume flat (uninformed) priors on this diffusivity field. The analysis presented above for a homogeneous (scalar) diffusivity then continues to hold.

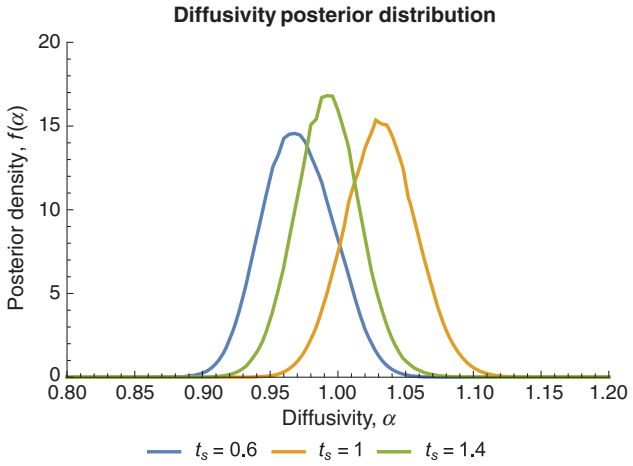

Figure 9. The posterior distribution of the diffusivity α for a varying total injection time t_s. Refer to Figure 2 for the definition of t_s.

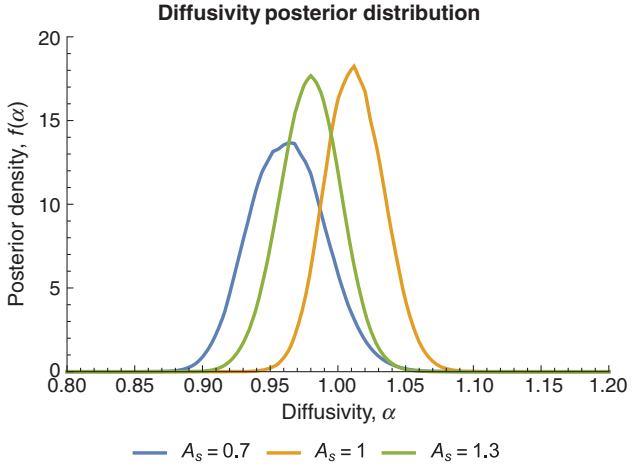

Figure 10. The posterior distribution of the diffusivity α for a varying injection rate A_s. Refer to Figure 2 for the definition of A_s.

The posterior distributions $f(\alpha_1, \alpha_2 | t_1, \ldots, t_N)$ of the diffusivity field given observed microseismicity for uncertainties in the minimum principal stress of 5%, 10%, and 20% are shown in Figures 12–14, respectively. We see in the left panels of these figures how a larger uncertainty in the minimum stress results in a larger variation of locations and occurrence times of microseismic events due to a larger variation in the effective stress. Inverting these microseismic data produces estimates of near- and far-well diffusivities α_1 and α_2 that carry uncertainties that increase with increasing uncertainty in σ_3.

EVENT LOCATION UNCERTAINTY

In this section, we complete our model by including the uncertainty in microseismic event locations that is always present in monitoring applications. Microseismic event locations and origin times are not observed directly. Instead, they are estimated with some uncertainty from recorded microseismic data (Michaud et al., 2004; Bennett et al., 2005; Huang et al., 2006; Poliannikov et al., 2013, 2014).

We denote by T the observed traveltime data, α the unknown diffusivity, and s the true microseismic event locations and origin times. Then we have

$$\begin{aligned} f(\alpha|T) &= \int f(\alpha, s|T)\mathrm{d}s \\ &= f^{-1}(T) \int f(T|\alpha, s) f(\alpha, s)\mathrm{d}s. \end{aligned} \tag{20}$$

It follows from the physics of the problem that $\alpha \to s \to T$; i.e., the diffusivity affects the observed traveltimes only through microseismic events that are triggered by diffusing pressure. Therefore,

$$f(T|\alpha, s) = f(T|s). \tag{21}$$

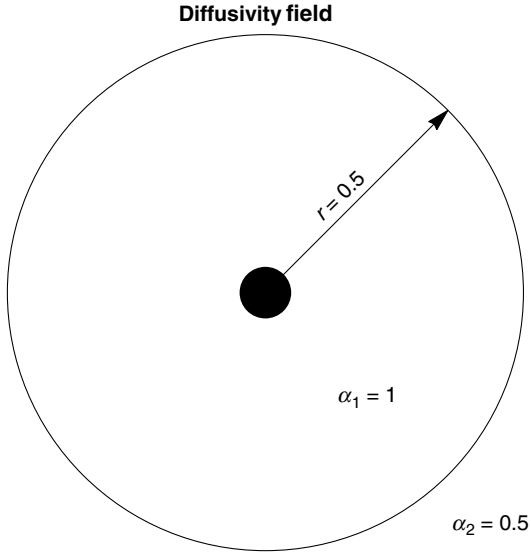

Figure 11. A nonhomogeneous diffusivity that assumes one value near the borehole and another value away from the borehole.

Substituting equation 21 into equation 20, we get

$$f(\alpha|T) = f^{-1}(T)\int f(T|s)f(\alpha,s)\mathrm{d}s$$
$$= f^{-1}(T)\int\left[\frac{f(s|T)f(T)}{f(s)}\right][f(\alpha|s)f(s)]\mathrm{d}s$$
$$= \int f(s|T)f(\alpha|s)\mathrm{d}s, \qquad (22)$$

where $f(s|T)$ is the probability density function of event locations *and* times, given the observed traveltimes, and $f(\alpha|s)$ is the posterior of diffusivity given microseismic events as computed in the previous section.

Studying the practical effects of uncertainty in the locations of microseismic events is deferred to future papers. It is clear that large uncertainty or biases in locations of individual events may adversely affect the uncertainty in the reconstructed diffusivity. Careful location uncertainty analysis that takes into account the experiment

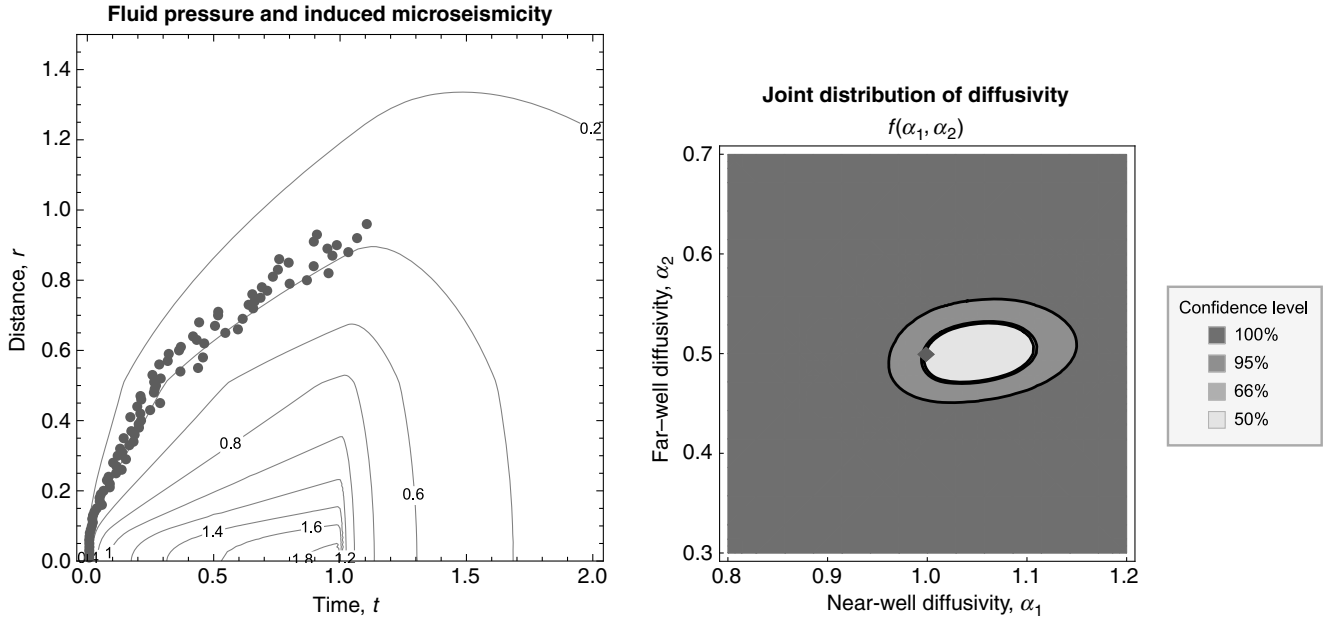

Figure 12. (a) Microseismicity realization for the diffusivity model shown in Figure 11 generated assuming known cohesion, friction, and maximum stress and allowing a 5% error in the minimum stress σ_3. The thin lines are isobars. (b) Uncertainty regions for the inverted diffusivity from the microseismicity shown in panel (a). The red diamond shows the true values of diffusivity.

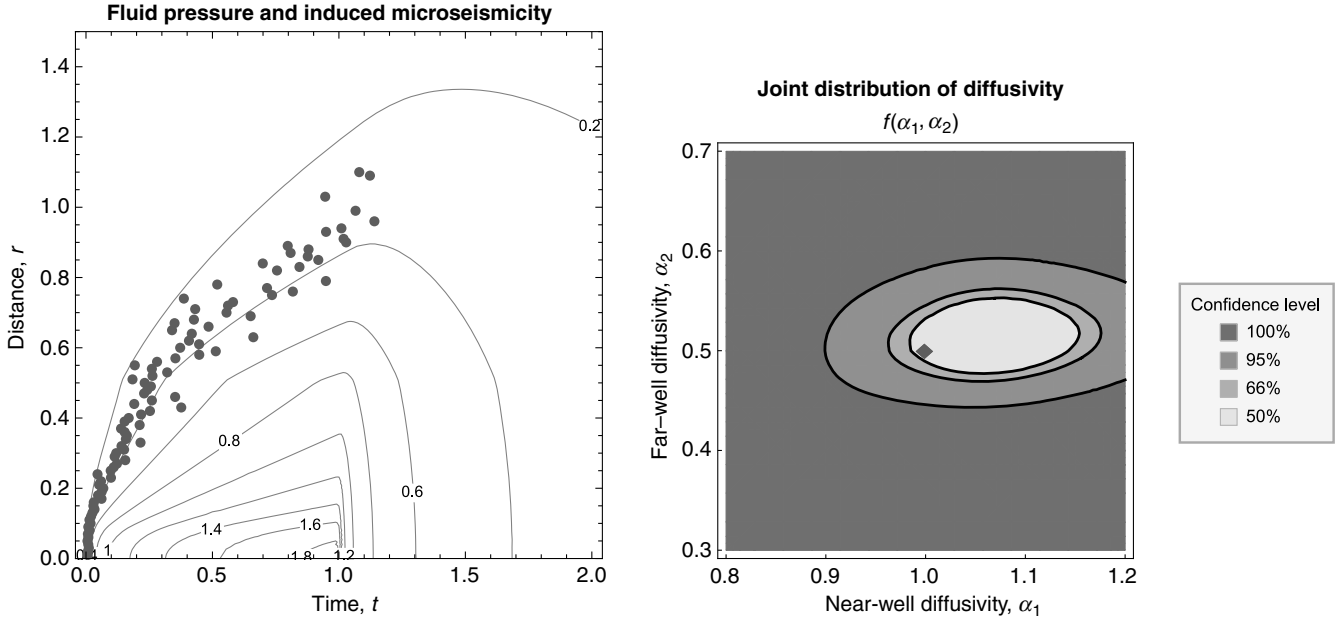

Figure 13. The same as Figure 12 but the uncertainty in σ_3 is 10%.

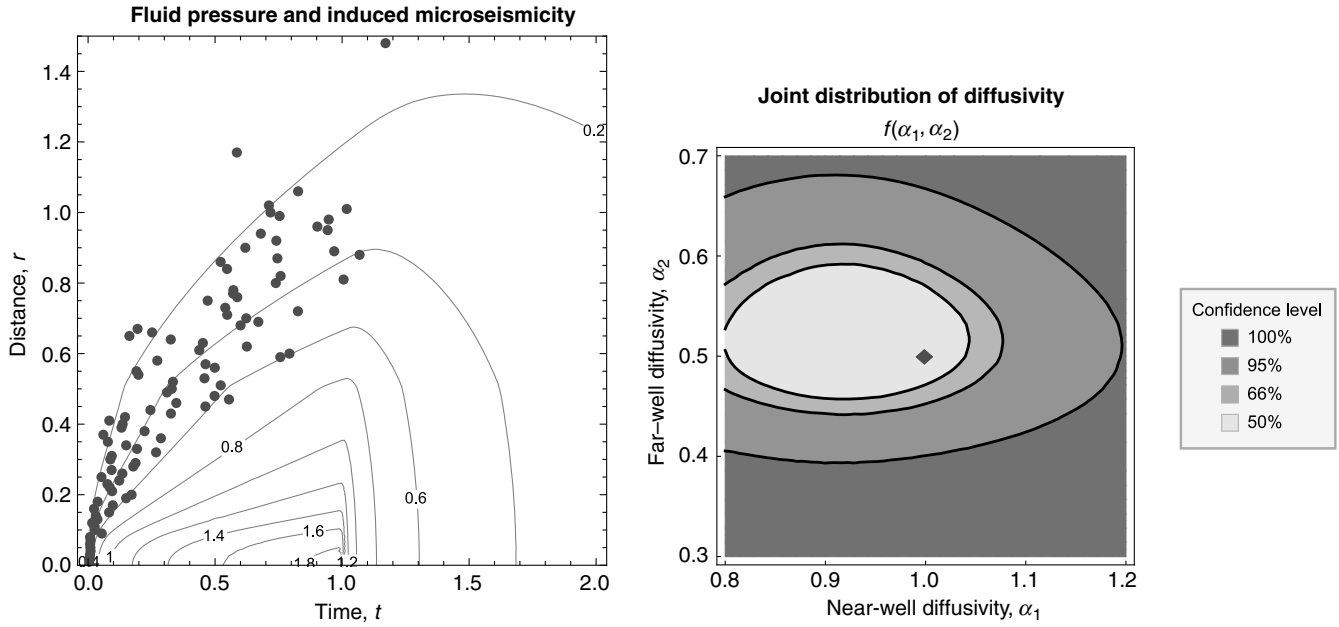

Figure 14. The same as Figure 12 but the uncertainty in σ_3 is 20%.

geometry, quality of the velocity model and other factors is necessary before a judgment can be made about whether or not microseismicity contains any reliable information about the flow in the subsurface.

DISCUSSION

This paper outlines a framework that includes several components. Each component of this framework could be considered and has been implemented as a separate module that could be modified at will depending on computational capability.

In this section, we touch upon several issues that are important for future theoretical work on this topic as well as for applying the proposed methodology in the field. One of the main limitations of the proposed probabilistic framework is that all events are assumed to be detected by the monitoring array. In practice, many events are not recorded due to low magnitude, a large source-receiver distance, or an unfavorable radiation pattern. Properly accounting for undetected events is an important topic for future research.

Another theoretical limitation is the assumption of the statistical independence of the geomechanical model parameters at different spatial locations. Including the spatial correlation between these model parameters is also a topic for future work. Note that including the correlation between model parameters at the same location induced by a known covariance matrix is completely straightforward.

Although we used a simple radially symmetric diffusive flow model and a simple Mohr-Coulomb failure model to build the forward model for predicting induced microseismicity, the probabilistic framework is much more general. This work elucidates the fundamental principles of determining flow parameters from induced microseismicity. Our flow model could be replaced with a full-scale reservoir simulator, and our fracture model could be enhanced by adding more parameters with the associated uncertainty. The basic principles of constructing a forward model and inversion would then remain unchanged, although the computational cost would rise quite significantly.

Our microseismicity prediction model concerns the fluid injection phase. To account for the back front (Parotidis et al., 2004), we would need to include repeated events at the same location.

The main value of this work is in the all-important risk assessment in microseismic monitoring (Djikpesse, 2015; O. V. Poliannikov and H. Djikpesse, personal communication, 2015). Fluid flow during the injection is ultimately tied to production, and any uncertainty at this stage will propagate forward in the production forecast. Quantifying uncertainty propagation between fluid flow and induced microseismicity, as well as in the inversion, is necessary for risk assessment in fracture design, survey design, and financial outcomes.

CONCLUSIONS

In this paper, we have shown that the fluid pressure during injection can be directly and physically related to the observed microseismic data. We have presented a relatively simple probabilistic model that captures the essential parameters that control fluid pressure, rock failure, and seismic wave propagation, and it can be used for forward predictions and inversions.

We also presented a probabilistic framework that allows rigorous uncertainty analysis. This analysis quantifies prediction and inversion errors, and it helps us find ways to improve the quality of predictions by identifying dependencies between uncertainties at different stages of the model.

We inverted for the effective diffusivity of the fracture system during injection, but it is unlikely that this diffusivity, inferred from microseismic data alone, will be adequate to forecast the fluid production capacity of the fracture system after the stimulation is complete. However, if a model of this type is used in conjunction with other types of data, such as pressure, temperature, production history, moment tensors, amplitudes, etc., then we may have a better

chance to forecast production and the associated quantities, such as fracture conductivity and stimulated volume.

ACKNOWLEDGMENTS

This work has been partially supported by the National Science Foundation, Division of Mathematical Sciences under grant no. 1115406.

REFERENCES

Bennett, L., J. L. Calvez, D. R. R. Sarver, K. Tanner, W. S. Birk, G. Waters, J. Drew, G. Michaud, P. Primiero, L. Eisner, R. Jones, D. Leslie, M. J. Williams, J. Govenlock, R. C. R. Klem, and K. Tezuka, 2005, The source for hydraulic fracture characterization: Oilfield Review, **17**, 42–57.

Charlez, P. A., 1997, Rock mechanics: Petroleum applications: Éditions Technip 2.

Cherian, B. V., J. M. Villalobos, R. D. Cooley, and M. L. Panjaitan, 2011, A multi-domain approach to understanding microseismic data in a tight gas play: Presented at Society of Petroleum Engineers Annual Technical Conference and Exhibition, 143975.

Djikpesse, H., 2015, C_{13} and Thomsen anisotropic parameter distributions for hydraulic fracture monitoring: Interpretation, **3**, no. 3, SW1–SW10, doi: 10.1190/INT-2014-0244.1.

Ground Water Protection Council; ALL Consulting, 2009, Modern shale gas development in the United States: A primer: Technical report, United States Department of Energy, Office of Fossil Energy and National Energy Technology Laboratory.

Huang, Y. A., J. Benesty, and J. Chen, eds., 2006, Acoustic MIMO signal processing: Time delay estimation and acoustic source localization: Springer, Signals and Communication Technology, 215–259.

Hummel, N., and S. A. Shapiro, 2013, Nonlinear diffusion-based interpretation of induced microseismicity: A Barnett Shale fracturing case study: Geophysics, **78**, no. 5, B211–B226, doi: 10.1190/geo2012-0242.1.

Jones, J. R., and L. K. Britt, 2009, Design and appraisal of hydraulic fractures: Society of Petroleum Engineers.

LaFollette, R. F., G. Izadi, and M. Zhong, 2013, Application of multivariate analysis and geographic information systems pattern-recognition analysis to production results in the Bakken light tight oil play: Presented at Society of Petroleum Engineers Annual Technical Conference and Exhibition, 163852.

Laplace, P. S., 1814, Théorie des probabilités: Ve. Courcier.

Maxwell, S., 2014, Microseismic imaging of hydraulic fracturing: Improved engineering of unconventional shale reservoirs, 1st ed.: SEG, Distinguished Instructor Series.

Michaud, G., D. Leslie, J. Drew, T. Endo, and K. Tezuka, 2004, Microseismic event localization and characterization in a limited aperture HFM experiment: 74th Annual International Meeting, SEG, Expanded Abstracts, 552–555.

Ottosen, N. S., and M. Ristinmaa, 2005, The mechanics of constitutive modeling: Elsevier.

Parotidis, M., S. A. Shapiro, and E. Rothert, 2004, Back front of seismicity induced after termination of borehole fluid injection: Geophysical Research Letters, **31**, L02612, doi: 10.1029/2003GL018987.

Poliannikov, O. V., M. Prange, A. E. Malcolm, and H. Djikpesse, 2013, A unified Bayesian framework for relative microseismic location: Geophysical Journal International, **194**, 557–571, doi: 10.1093/gji/ggt119.

Poliannikov, O. V., M. Prange, A. E. Malcolm, and H. Djikpesse, 2014, Joint location of microseismic events in the presence of velocity uncertainty: Geophysics, **79**, no. 6, KS51–KS60, doi: 10.1190/geo2013-0390.1.

Shapiro, S. A., P. Audigane, and J.-J. Royer, 2000, Reply to comment by F. H. Cornet on "Large-scale in situ permeability tensor of rocks from induced microseismicity": Geophysical Journal International, **140**, 470–473, doi: 10.1046/j.1365-246x.2000.00017.x.

Shapiro, S. A., S. Rentsch, and E. Rothert, 2005a, Characterization of hydraulic properties of rocks using probability of fluid-induced microearthquakes: Geophysics, **70**, no. 2, F27–F33, doi: 10.1190/1.1897030.

Shapiro, S. A., S. Rentsch, and E. Rothert, 2005b, Fluid-induced seismicity: Theory, modeling, and applications: Journal of Engineering Mechanics, **131**, 947–952, doi: 10.1061/(ASCE)0733-9399(2005)131:9(947).

Shapiro, S. A., E. Rothert, V. Rathz, and J. Rindschwentner, 2002, Characterization of fluid transport properties of reservoirs using induced microseismicity: Geophysics, **67**, 212–220, doi: 10.1190/1.1451597.

Suarez-Rivera, R., L. Behrmann, S. Green, J. Burghardt, S. Stanchits, E. Edelman, and A. Surdi, 2013a, Defining three regions of hydraulic fracture connectivity, in unconventional reservoirs, help designing completions with improved long-term productivity: Presented at Society of Petroleum Engineers Annual Technical Conference and Exhibition, 166505.

Suarez-Rivera, R., J. Burghardt, S. Stanchits, E. Edelman, and A. Surdi, 2013b, Understanding the effect of rock fabric on fracture complexity for improving completion design and well performance: Presented at International Petroleum Technology Conference.

Vincent, M., 2010, Refracs — Why do they work, and why do they fail in 100 published field studies?: Presented at Society of Petroleum Engineers Annual Technical Conference and Exhibition, 134330.

Vincent, M., 2012, The next opportunity to improve hydraulic-fracture stimulation: Journal of Petroleum Technology, **64**, 118–127, doi: 10.2118/144702-JPT.

Von Terzaghi, K., 1943, Theoretical soil mechanics: John Wiley & Sons, Ltd.